ACS APPLIED MATERIALS & INTERFACES

Research Article

www.acsami.org

Interfacial Load Transfer in Polymer/Carbon Nanotube Nanocomposites with a Nanohybrid Shish Kebab Modification

Min Nie,[†] Dilhan M. Kalyon,[‡,§] and Frank T. Fisher*[,†]

[†]Department of Mechanical Engineering, [‡]Department of Chemical Engineering and Materials Science, and [§]Department of Chemistry, Chemical Biology and Biomedical Engineering, Stevens Institute of Technology, Hoboken, New Jersey 07030, United States

ABSTRACT: Interfacial properties are known to have a critical effect on the mechanical properties of a nanocomposite material system. Here, the interfacial load transfer in a carbon nanotube (CNT)/nylon-11 composite was studied with a CNT/nylon-11 nanohybrid shish kebab (NHSK) structure modification using Raman spectroscopy. Characterization of the polymer crystal in the NHSK using differential scanning calorimetry (DSC) for the first time indicates that the NHSK structure formed a more perfect crystal structure than the bulk polymer. On the basis of transmission electron microscopy and DSC results, a new growth model for the NHSK crystal is hypothesized, indicating the formation of an initial uniform crystal layer on the CNT prior to the crystallization of the kebabs. Characterization of the nanocomposites using Raman spectroscopy, with the samples heated to introduce interfacial shear stress caused by thermal expansion mismatch, found that the D* band of the CNT in the NHSK/nylon-11 composite displayed a more pronounced shift with an increase in temperature, which is attributed to the NHSK structure being more effective at transferring load from the nylon matrix to the nanotube inclusions. The NHSK structure was also used to fabricate composites with two amorphous polymers, polycarbonate and poly(methyl methacrylate), to investigate the load transfer mechanism. It was found that when the compatibility between the polymer in the NHSK structure and the bulk polymer matrix at the molecular level is sufficiently high, the ensuing mechanical interlocking effect further enhances the interfacial load transfer for polymer nanocomposites. Additional mechanical characterization of polymer nanocomposites with 0.1 wt % NHSK reinforcement demonstrates how the moduli and ultimate tensile strength of the nanocomposites can be improved via this NHSK structure.

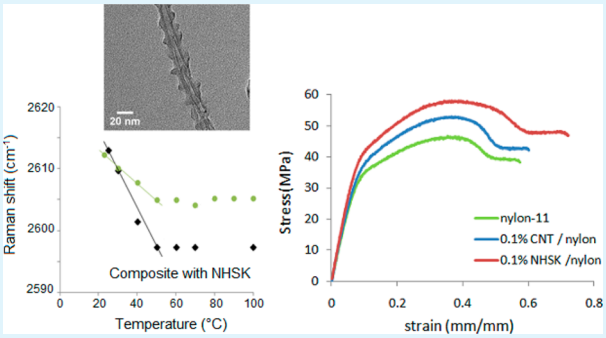

KEYWORDS: *interfacial load transfer, nanohybrid shish kebab (NHSK), NHSK growth mechanism, carbon nanotubes, semicrystalline polymers, nylon-11*

1. INTRODUCTION

In recent years carbon nanotubes (CNTs) have been pursued as a promising nanoreinforcement material to enhance the properties of polymeric materials, even at very small loadings of the nanotube reinforcement.[1−5] In all polymer nanocomposite material systems, the interfacial shear stress is a critical factor in determining the effectiveness of load transfer between the polymer matrix and the nanoreinforcement inclusion phase. One common approach to enhance the interfacial bonding between the embedded CNTs and a polymer matrix is chemical functionalization, a process which purposefully creates defects on the nanotube surface to generate active functional groups on the nanotubes which can then be covalently bonded with polymer chains.[1−4] However, the chemical functionalization inherently creates defects in the CNT structure, which necessarily degrades the properties of the nanotubes and subsequently reduces the effective properties of the entire composite.

Recently, Li et al.[6−9] developed a new hybrid structure of carbon nanotubes decorated with polymer nanocrystals, which they referred to as the nanohybrid shish kebab (NHSK) structure. It was found that certain crystallizable polymers such as polyethylene (PE) and nylon-6,6 formed periodic, disk-shaped crystals on the nanotube surface.[6−13] While this earlier work with the NHSK structure showed that the formation of this structure is closely related to the regular atomic arrangement of the CNT surface, the details of the growth mechanism of the NHSK structure were not fully investigated. In the current work, through differential scanning calorimetry (DSC) and transmission electron microscopy (TEM) analysis, a two-step crystallization model is provided to further reveal the details in the CNT/nylon NHSK formation process.

With the surface of the CNT fully covered by the periodic kebab crystals consisting of the aligned polymer chains, the decorated NHSK structure has a rougher surface to enhance the interfacial interaction between the CNTs and the polymer

Received: March 27, 2014
Accepted: August 19, 2014
Published: August 19, 2014

matrix. On the basis of this principle, the NHSK nanostructure is able to provide a non-covalent method for the enhancement of the interfacial interactions between carbon nanotubes and the polymer matrix without sacrificing the mechanical properties of the carbon nanotubes.

However, the interfacial shear stress is extremely difficult to measure when the filler size decreases to the nanoscale.[14−16] One of the effective ways of measuring the interfacial load transfer between carbon nanotubes and the polymer is through Raman spectroscopy. The Raman scattering signal for the embedded carbon nanotube is much stronger in comparison to that of the polymer due to the resonance-enhanced Raman scattering effect. This makes Raman spectroscopy an outstanding tool to detect the effective mechanical deformation of embedded carbon nanotubes when the composites are deformed, which is used here to study the interfacial shear stress between the polymer and carbon nanotube. The relationship between CNT deformation and the shift of the CNT Raman response is well-known, where the D* peak in the Raman spectrum shifts to a lower wavenumber when the CNTs are in tension along the longitudinal direction.[17−29]

In most cases, an external force was applied to stretch the sample and a peak-shifting trend was observed. For example, Zhao et al.[17] studied the relation between the Raman shift and the applied load in a CNT/polyurethane acrylate composite. Liu et al.[18] coated glass fibers with CNT/epoxy composite and studied the shift of the G′ band (also referred to as the D* band) corresponding to the axial strain of the glass fibers. However, for a bulk nanocomposite sample with randomly distributed CNTs subjected to an applied external force, Raman is not able to reflect the strain of the CNTs in the direction of the applied load. This requires that either the CNTs are aligned during the fabrication process or polarized Raman spectroscopy is used to eliminate the influence of the distribution of CNTs within the nanocomposite.[19−21] To overcome this challenge, we developed an alternative experimental Raman method that is based on the mismatch of the coefficient of thermal expansion between the CNTs and the polymer matrix during sample heating to generate interfacial shear stress in a nanocomposite sample. This stress induces a local tensile force to the CNT, which causes a peak shift of the D* Raman band and is used to characterize the interfacial load transfer in the nanocomposite.

To illustrate the impact of the NHSK structure on load transfer within a polymer nanocomposite, nylon-11 is used in this work. Nylon-11 is a semicrystalline polymer that exhibits piezoelectric and ferroelectric properties and is often studied for actuator and sensor applications. Here the introduction of the NHSK structure in the composite is expected to enhance the mechanical properties of nylon-11 to broaden the potential applications of this polymer. Two other polymers, poly(methyl methacrylate) (PMMA) and polycarbonate, were also used to study the mechanism of the reinforcing effects of NHSK as discussed below. In addition to the Raman characterization of the load transfer behavior in these nanocomposites, complementary mechanical characterization further demonstrates how the macroscale effective properties of the nanocomposites can be improved via this novel NHSK structure.

2. EXPERIMENTAL SECTION

2.1. Materials, NHSK, and Nanocomposite Fabrication. Nylon-11 (polyamide-11, MW 18 000) pellets, polycarbonate (MW 60 000) pellets, and poly(methyl methacrylate) (MW 540 000) powder were purchased from Scientific Polymer Products, Inc. Multiwall carbon nanotubes (purity >95 wt %) with an outer diameter of 20−30 nm and a length of approximately 10−30 μm were purchased from Cheap Tubes Inc. 1,4-Butanediol (BDO) (Fluka, purity >98.8% by GC) was used as the solvent for dissolving nylon-11 and dispersing the carbon nanotubes. Phosphoric acid (85%) was purchased from Fisher Scientific.

The fabrication of the CNT/nylon-11 NHSK structure was as follows. First, 3.2 mg of nylon-11 was dissolved in 16 mL of 1,4-butanediol at 165 °C to form a 0.02% solution. Separately, 0.8 mg of multiwall carbon nanotubes were dispersed in 4 mL of 1,4-butanediol by sonication for 10 min to form a 0.02% suspension. At a weight ratio of 1:4 between the CNTs and polymer, the two dispersions were mixed and annealed at 147 °C for 30 min to 1 h. Initially, during sonication, the dispersions were stable due to charge on the nanotube surface. As the NHSK crystallites formed and grew, the additional polymer started to shield the surface charge, which allowed agglomerates to form. The resulting NHSKs were then filtrated isothermally and washed with acetone prior to the characterization described below. A key benefit of using nylon-11 here is that a slower rate of crystallization results in a very small amount of residual polymer crystallizing outside the NHSK structure during filtration. This enables us for the first time to conduct a detailed DSC analysis of the NHSK structure without the signal being masked by the response of the pure polymer crystals.

To fabricate a 0.1% NHSK/nylon-11 composite, 4 times the amount of NHSK aggregates in BDO obtained from the previous step were sonicated for 10 min to disperse the NHSK. The uniform NHSK suspension was then heated at 147 °C for 10 min and added to a 3−5% nylon solution in BDO dissolved at 165 °C. The mixture was stirred and slowly cooled, during which the composite crystal precipitated out. Three times the volume of isopropyl alcohol was then added, after which the precipitate was collected by vacuum filtration and dried in a vacuum oven to remove residual solvent. The resulting gray nanocomposite powder was molded under a pressure of 550 psi and a temperature of ∼195 °C to form ∼0.1 mm thin film samples and ∼1 mm dogbone-shaped bulk nanocomposite samples for further characterization. For comparison, 0.1% CNT/nylon-11 composite samples (without the NHSK structure) were fabricated by directly adding the original CNT suspension into the nylon-11 solution prior to precipitation of the nanocomposite while maintaining the other steps described above. Samples fabricated in this way were used as a control.

In addition, two amorphous polymers, PMMA and polycarbonate, were also used to form composites following a similar solution precipitation method. For the fabrication of the NHSK/PMMA samples, acetone was used as the solvent and distilled water as the anti-solvent. For the fabrication of NHSK/polycarbonate samples, methylene chloride and ethanol were used as the solvent and anti-solvent, respectively. PMMA and polycarbonate samples were molded under a pressure of 550 psi and a temperature of 180 °C. Control samples with the NHSK reinforcement replaced by as-received CNTs were fabricated using an identical procedure.

2.2. Scanning Electron Microscopy (SEM) and TEM. The NHSK samples were characterized using a field emission scanning electron microscope (Auriga, Carl Zeiss NTS GmbH, Germany) with an acceleration voltage of 1 kV and a transmission electron microscope (FEI CM20) with an acceleration voltage of 200 kV. For SEM imaging, the NHSK samples were placed on a silicon substrate and sputtered with gold to reduce overcharging.

2.3. DSC. The melting and crystallization behavior of bulk polymer, the fabricated NHSK structures, and the composite samples were characterized using differential scanning calorimetry (DSC Q100, TA Instruments, New Castle, DE). The samples were heated at 10 °C/min from 25 to 230 °C, held isothermally for 0.5 min, and then cooled at 10 °C/min to 25 °C under a nitrogen environment with a nitrogen gas flow rate of 50 mL/min.

2.4. Raman Spectroscopy. Both pure carbon nanotubes and nanocomposite samples were tested using a Raman Spectrometer (Nicolet Almega XR Dispersive Raman spectrometer, Thermo Scientific, Madison, WI) equipped with a 780 nm wavelength laser

which has 100% laser power of 12 mW. For characterization of the Raman response as a function of temperature, a 2 in. × 2 in. heating element (McMaster, ultrathin heat sheet, KH-2X2-10-115A, 10 W/in^2) and a digital temperature controller (AutomationDirect.com, model SL4824-RR) connected with a type J thermocouple were used. The heating element was fastened between glass slides and an aluminum plate. Temperatures from 20 to 230 °C with a resolution of 0.1 °C were achievable using this setup. In the tests at room temperature, CNT and nylon nanocomposite samples were excited with 80−100% laser power. Each test accumulates the signal for 6 min, with an exposure time of 5 s and the number of scans set to 72. In tests to observe the Raman response as a function of temperature, 50% laser power was used to excite the nanocomposites at high temperature to avoid ablation damage of the sample. For this reason, the accumulation time was also reduced to 1 min with an exposure time of 5 s for the 12 scans. To ensure uniform isothermal conditions at different temperatures, before each Raman test the samples were maintained at the constant test temperature for about 20 min. Both 0.1 mm thin films and 1 mm thick samples were tested.

2.5. Mechanical Characterization. Tensile tests were performed with a tensile test machine (Instru-met Corp.). Tensile test samples obtained from the above composite fabrication steps had a nominal gauge length of 10 mm, a width of 3.5 mm, and a thickness of 1 mm. The samples were loaded in constant deformation mode at a speed of 5 mm/min. Three samples were used for each test.

3. RESULTS AND DISCUSSION

Figure 1 shows the SEM images of the as-received carbon nanotubes and the nanohybrid shish kebab structure on silicon.

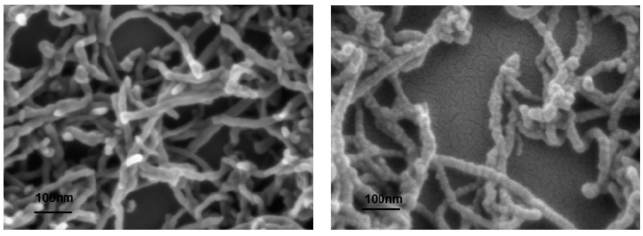

Figure 1. (Left) SEM image of CNTs and (right) nanohybrid shish kebabs of nylon-11 on CNTs. The scale bar represents 100 nm.

The periodic nylon-11 crystal structure can be seen to cover all the carbon nanotubes. As shown in Figure 2, TEM images further reveal the finer structure of the kebab crystals that has a thickness gradient from the outer to the inner rim. Figure 3 shows the structure obtained after the NHSK is etched by 85% H_3PO_4 at 120 °C for 30 min. An approximately 2 nm crystal layer of polymer remains on the CNT, which indicates a difference in the etch rate of the kebab versus the underlayer of the kebabs of the NHSK crystal structure. Such results are consistent with the DSC characterization of the NHSK structure and are further interpreted below.

3.1. Differential Scanning Calorimetry Characterization. The heating and cooling curves in DSC for the various samples are shown in Figure 4, and the results for the heat of melting are summarized in Table 1. The pure nylon-11 was observed to have a melting point at 191 °C and a crystallization point at 155 °C. The composite directly fabricated with CNTs (CNT/nylon-11) had an endothermic heat of 46.2 J/g at a melting point of 190 °C. By comparison, the molded 0.1% NHSK/nylon-11 sample had approximately the same melting point, but a higher endothermic heat of melting of 54.2 J/g, compared to 41.0 J/g for the pure nylon-11 sample.

The change of the heat of melting and crystallization of the polymer indicates a difference in the crystal structure and

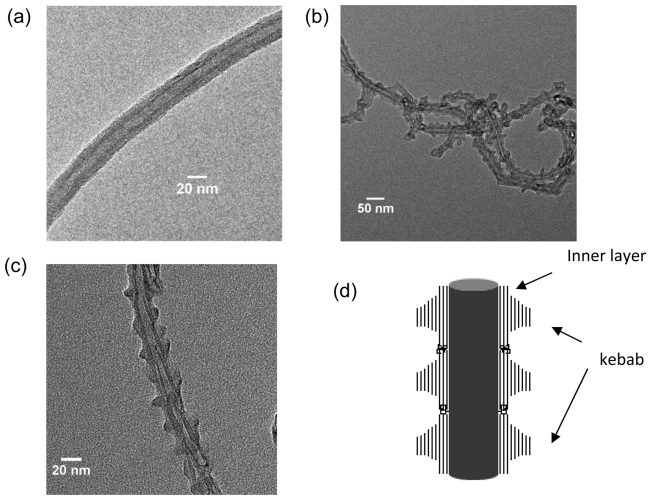

Figure 2. (a) TEM image of an as-received CNT. (b, c) TEM images of nanohybrid shish kebabs fabricated from nylon-11 and CNTs at different magnifications. (d) Schematic of the nanohybrid shish kebab structure.

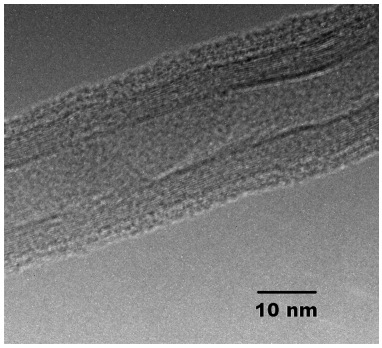

Figure 3. TEM image of the structure obtained after the nanohybrid shish kebabs are etched in H_3PO_4 at 120 °C for 30 min. The thickness of the remaining polymer underlayer is about 2 nm.

crystallinity of the nylon polymer caused by the NHSK structure. It is inferred from the heat of melting that the nucleating activity of the NHSK substantially increased the crystallinity of the nylon polymer, while when using the bare CNT the enhancement of crystallinity was less pronounced. During the cooling process, the heat of crystallization results show similar values for the pure nylon polymer and CNT/nylon-11 and NHSK/nylon-11 composites. However, the crystallization temperature of the CNT/nylon-11 and NHSK/nylon-11 nanocomposites increased from 155 to 168 and 171 °C, respectively, due to the enhanced nucleation within the nylon-11 matrix. In comparison, for the NHSK/PMMA and NHSK/polycarbonate samples, DSC results (not shown) confirm the same glass transition temperatures as the control samples fabricated with the as-received CNTs, indicating that the NHSK structure does not significantly affect the amorphous phase of these two polymers in the composites.

From the results in Figure 4, the heating curve for the nylon-11 NHSK samples interestingly showed two peaks at 197 and 205 °C, respectively. It is known that the melting point of a polymer crystal is dependent on the thickness of the lamella, with a higher melting point indicating a thicker lamella size. For example, for a polymer crystal in the shape of a cylinder, it has been shown that[30]

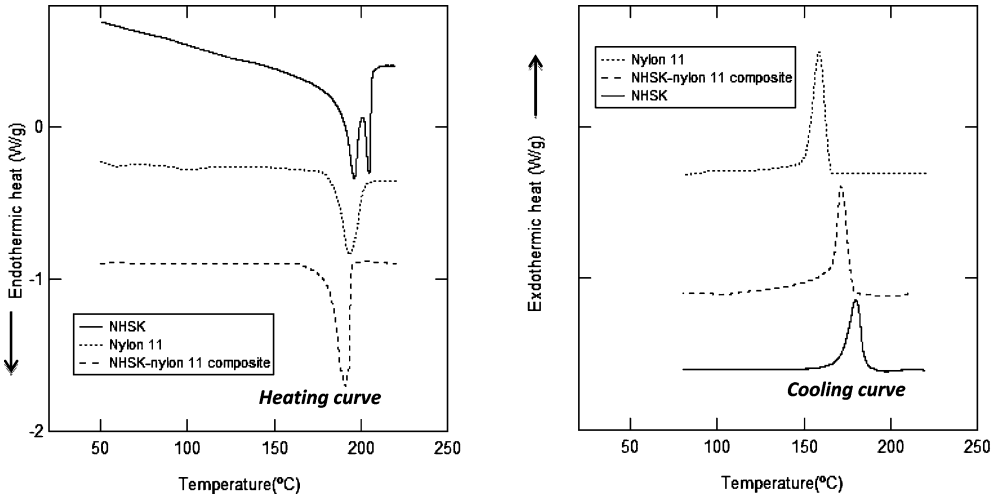

Figure 4. (Left) Heating and (right) cooling curves for pure nylon-11, the CNT/nylon-11 NHSK structure, and the NHSK/nylon-11 composite using DSC.

Table 1. Heat of Melting of Different Samples

sample	heat of melting (J/g)
nylon-11	41.0
CNT/nylon-11 powder	66.6
CNT/nylon-11 molded sample	46.2
NHSK/nylon-11 powder	75.5
NHSK/nylon-11 molded sample	54.2

$$T_m = T_m^\infty - \frac{2\gamma}{\Delta H_V^\infty}\left(\frac{1}{l} + \frac{1}{r}\right)T_m^\infty \quad (1)$$

where T_m^∞ is the ideal melting point of the crystal with infinite dimensions, ΔH_V^∞ is the enthalpy change of the crystal with infinite dimensions in unit volume, γ is the Gibbs free energy per area of the interface, and r and l are the radius and thickness of the polymer crystal, respectively. The two melting points in the DSC results for the NHSK are both higher than those of the pure nylon sample, suggesting that thicker crystals are formed in the NHSK sample, which will provide more effective mechanical reinforcement for the composite. The presence of the two melting points also indicates that the polymer crystal on the NHSK includes two sizes of lamellae, which is a phenomenon that has not been reported previously in the NHSK literature.

On the basis of the structure of a pure polymer "shish kebab",[31] which consists of periodic parallel disks crystallized on an inner fiber containing extended polymer chains, it is hypothesized that the NHSK has an analogous uniform underlayer crystal epitaxially grown on the CNT surface before the kebabs. As shown in Figure 4, of the two endothermic peaks for the NHSK structure, the crystal phase with the lower melting point displays a larger volume fraction and broader peak distribution than the crystal phase with the higher melting point. These observations are consistent with the hypothesized NHSK structure (Figure 2d), including kebabs with a thickness gradient and a uniform underlayer crystal as observed in the TEM image in Figure 3. Since the inner layer crystal with the higher melting point has a relatively small radial thickness, estimated to be about 2 nm, compared to the kebab radial thickness of about 7 nm, the inner layer should have the larger lamella thickness in the longitudinal direction to enable the higher melting temperature. This suggests that the NHSK structure is formed in the following sequence: a uniform layer of periodic polymer crystals separated by an amorphous phase is first formed on the CNT surface, and then the kebabs are further crystallized on this periodic polymer crystal underlayer.

It was also found that when the annealing temperature was decreased from 147 to 141 °C, the two melting points decreased from 197 and 205 to 194 and 202 °C, respectively. The two melting points have decreased by the same extent, indicating the two lamella sizes are correlated and the kebab lamella thickness is dependent on the inner layer lamella thickness in the longitudinal direction.

3.2. Raman Spectroscopy Characterization. Raman spectroscopy was used to characterize the interfacial load transfer in the nanocomposite samples based on the strains imposed on embedded CNTs by the mismatch of the thermal expansion coefficients between the polymers and the CNTs during the heating process. Since the laser spot diameter is only 3.1 μm, within a certain penetration depth only a limited number of carbon nanotubes are probed to reflect the strain change of the local CNTs. As discussed previously, it is known that a shift of the D* Raman band to a lower wavenumber corresponds to a tensile strain applied to the CNTs.[17−29] Since during the heating process in the current there was no external force applied on the sample, the strain of the CNTs was caused solely by the thermal expansion mismatch within the nanocomposite. The coefficient of thermal expansion (CTE) for a polymer is usually 2 or 3 orders of magnitude higher than that of the CNTs. The CTE of the carbon nanotubes is estimated to be on the order of 10^{-6} K^{-1},[32] while the CTE of nylon-11 is on the order of 10^{-4} K^{-1}.[33] Therefore, when the temperature is raised, there is a mismatch between the thermal expansion of the embedded carbon nanotubes and nylon-11 polymer, an effect which is used to apply strain to the CNTs in the absence of an external applied force. A distinct advantage of the thermal expansion approach used here is that it is able to strain the embedded nanotubes independent of the direction of the CNTs, whereas applying an external force to strain the embedded CNTs requires the alignment of carbon nanotubes with respect to the direction of the applied load or the use of polarized Raman spectroscopy. In separate tests, free-standing pure carbon nanotube samples (with no polymer) did not experience a Raman peak shift when heated from 25 to 100 °C,

as the thermal expansion mismatch is not a factor for pure nanotubes without a polymer matrix.

The Raman spectra of pure nylon-11, as-received carbon nanotubes, and NHSK/nylon-11 composites at room temperature are shown in Figure 5. In the 0.1% nanocomposite the D* band of the CNTs can be distinguished from the bands of nylon to be used in characterizing the strain of the CNTs in the nanocomposites. In addition to Raman characterization at room temperature, the nanocomposite samples were characterized at temperatures ranging from room temperature (approximately 25 °C) to 100 °C, where the mismatch in CTE results in strain induced in the embedded nanotubes. As shown in Figure 6, the D* band of Raman spectra for the 0.1% CNT/nylon-11 composite shifted from higher to lower wavenumber with increasing temperature, while above a certain temperature the peak position appears to remain stable. During an approximately 25 °C change in temperature, the Raman D* band of the CNTs in the NHSK/nylon-11 composite has shifted 16 cm^{-1} to a lower wavenumber, while in the control composite with the as-received CNTs the corresponding shift was only 8 cm^{-1}. The nanocomposite with the NHSK structure had a steeper slope of wavenumber change as a function of temperature. This indicates that the larger strains exhibited by the CNTs in the case of the NHSK nanocomposite due to the enhanced load transfer were enabled by the presence of the NHSK structure.

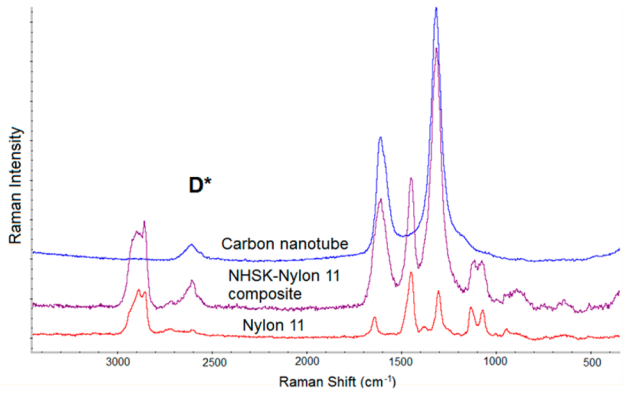

Figure 5. Raman spectra of nylon-11, CNTs, and the NHSK/nylon-11 composite at room temperature.

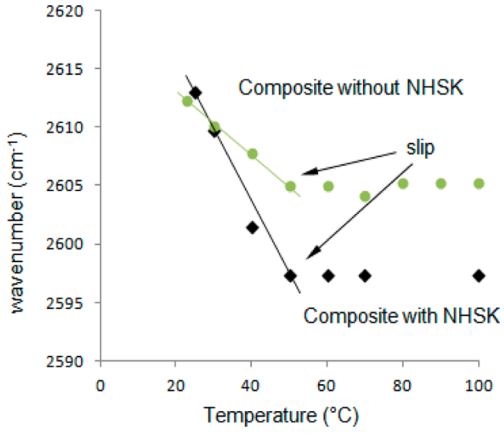

Figure 6. D* band (~2600 cm^{-1}) shift of the CNTs in CNT/nylon-11 composites fabricated with and without the NHSK structure.

It is also observed in Figure 6 that at a certain temperature there is a sudden change in the D* band (~2600 cm^{-1}) Raman response of the samples, which transitions from a linear decrease as a function of temperature to a constant wavenumber independent of temperature, which we refer to as "slip". This transition from peak shifting of the D* band at lower temperatures to a constant wavenumber of the peak position at higher temperatures can be attributed to the glass transition of the bulk nylon-11 in a manner similar to what has been described for the amorphous polymers polycarbonate and polyurethane acrylate in the previous literature.[22] The constant wavenumber suggests that the semicrystalline polymer still has sufficient strength to hold the stress of the CNTs above T_g because of the high crystallinity.

Comparing the Raman results in current work with those for amorphous polymer/CNT composites of polycarbonate and polyurethane acrylate described in the literature, although the two polymers have thermal expansion coefficients (65×10^{-6} and 110×10^{-6} K^{-1}) similar to that of nylon-11 (100×10^{-6} K^{-1}), the shifting rates of their wavenumber were both less than 0.1 cm^{-1} $°C^{-1}$. On the other hand, in the current work we have observed wavenumber shifts of the D* band of 0.32 cm^{-1} $°C^{-1}$ for the as-received CNTs and 0.64 cm^{-1} $°C^{-1}$ for the NHSK nanocomposite over a 25 °C change in temperature. While the lower modulus of polyurethane acrylate might partially account for the smaller level of strain experienced by the carbon nanotubes in the earlier work, the primary reason for the larger strain in the CNT/nylon-11 composite observed here is attributed to the stronger interaction between CNTs and nylon when nylon is crystallized on the CNTs. In addition, for the NHSK/nylon-11 composite samples, with the formation of the NHSK structure the interfacial area between the crystallized nylon and CNTs was substantially increased, which further improves the interaction between the CNTs and the nylon matrix and results in a more dramatic shifting of the Raman peak in comparison to that of the CNT/nylon-11 composite.

To further understand how the NHSK structure improves the nanocomposite interface, the CNT/nylon-11 NHSK nanostructure was also applied in the fabrication of two amorphous polymer composites: NHSK/polycarbonate and NHSK/PMMA. The Raman response of these composites as a function of temperature is shown in Figures 7 and 8. For the

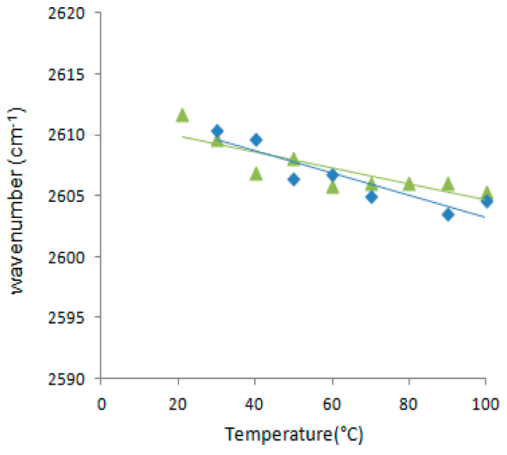

Figure 7. D* band shift in CNT/polycarbonate composites fabricated with (green) and without (blue) the NHSK structure. The minimal difference in slope between the samples is attributed to poor compatibility between the nylon-11 and the polycarbonate.

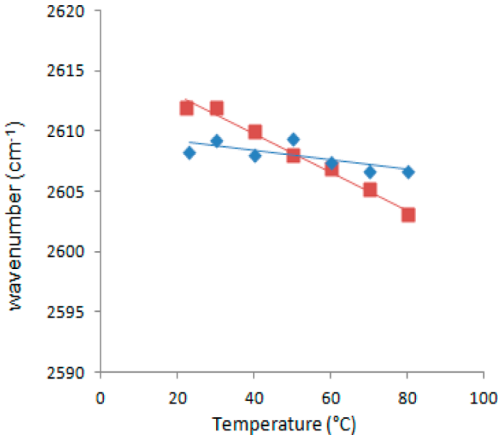

Figure 8. D* band shift in CNT/PMMA composites fabricated with (red) and without (blue) the NHSK structure. The difference in slope between the samples is attributed to sufficient compatibility between the nylon-11 and the PMMA to facilitate an interlocking effect caused by the NHSK structure.

polycarbonate composites, the NHSK structure does not show a significant enhancement of the interfacial load transfer on the basis of the Raman peak shift (Figure 7). This is attributed to the difference of the compatibility between the two polymers (nylon-11 in the NHSK structure and the polycarbonate matrix) and that between the polycarbonate and CNTs. It is known that polycarbonate and nylon are incompatible polymers when they are blended, but the structure of the benzene ring in polycarbonate (Figure 9) enhances the compatibility between polycarbonate and the CNTs due to molecular interaction of $\pi-\pi$ stacking. Therefore, when the nylon NHSK was embedded in the polycarbonate matrix, the effect of molecular level incompatibility partially offset the interlocking effect on the interfacial load transfer.

On the other hand, for the NHSK/PMMA composite, the NHSK structure exhibits a distinctly positive effect on the interface. Figure 8 shows the result of the Raman peak shift of NHSK/PMMA and CNT/PMMA composites as a function of temperature from room temperature to 80 °C. In this range, the shifting rate of the Raman band for the NHSK/PMMA sample has clearly increased compared to that of the control sample, indicating that the interface in the NHSK/PMMA sample is stronger than that in the CNT/PMMA sample. Although the molecular interaction between PMMA and nylon is not substantially high,[34] here it is sufficient to facilitate the interlocking effect caused by the NHSK structure. Therefore, the enhancement of the interfacial load transfer in the NHSK/PMMA samples can be attributed to two major factors: the adequate compatibility between PMMA and nylon-11 and the interlocking effect between the NHSK and the PMMA matrix. The results from NHSK/amorphous polymer composites prove that when the molecular compatibility between the polymer matrix and the modifying polymer is sufficiently high, the mechanical interlocking effect provides an additional mechanism to further enhance the interfacial load transfer between the CNTs and the polymer matrix.

3.3. Mechanical Characterization. Tensile tests of the three pure polymers and their composites with CNT or NHSK reinforcement show that the effective mechanical properties of the samples can be significantly improved via the incorporation of small amounts (0.1 wt %) of the NHSK structure. Figure 10

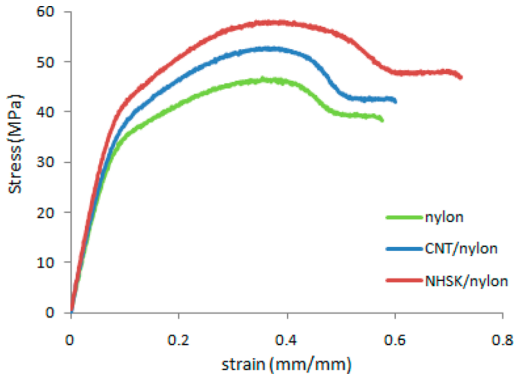

Figure 10. Stress–strain curves of pure nylon, CNT/nylon, and NHSK/nylon samples.

shows the stress–strain curves for the pure nylon, CNT/nylon, and NHSK/nylon samples. The pure nylon-11 sample has a Young's modulus of 493 MPa and an ultimate tensile strength of 46.7 MPa. The CNT/nylon composite has a Young's modulus of 538 MPa and an ultimate tensile strength of 52.9 MPa. In comparison, the NHSK/nylon composite has a Young's modulus of 586 MPa and an ultimate tensile strength of 59.1 MPa. From Figure 10, it is also clear that the NHSK/nylon sample is able to maintain a higher stress over a wider range of strain than the control sample, which indicates an enhanced interface resulting from the NHSK reinforcement as compared to the as-received carbon nanotubes.

The stress–strain curves for the polycarbonate, CNT/polycarbonate, and NHSK/polycarbonate samples are shown in Figure 11. The Young's moduli of polycarbonate, CNT/polycarbonate, and NHSK/polycarbonate are 718, 735, and 791 MPa, respectively, while the ultimate tensile strengthes are 63.1, 64.7, and 65.8 MPa, respectively. At higher strains as the samples neck, the NHSK/polycarbonate composite maintains a higher stress enabled by the interlocking effect of the NHSK structure. However, the molecular compatibility of the NHSK/polycarbonate sample results in a decrease in the ultimate strain. These results are consistent with the Raman results in which D* bands have a similar slope for both nanocomposites.

For the PMMA samples shown in Figure 12, the Young's modulus of NHSK/PMMA is increased to 1239 MPa compared with 1031 MPa for PMMA and 1107 MPa for

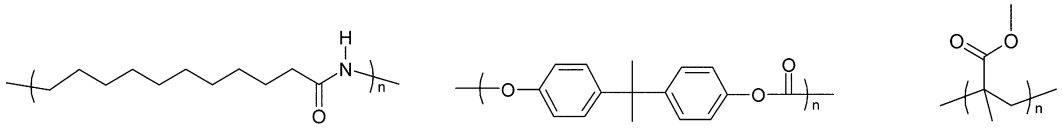

Nylon-11 Polycarbonate Poly(methyl methacrylate)

Figure 9. Chemical structures of three polymers.

dx.doi.org/10.1021/am501879q | ACS Appl. Mater. Interfaces 2014, 6, 14886–14893

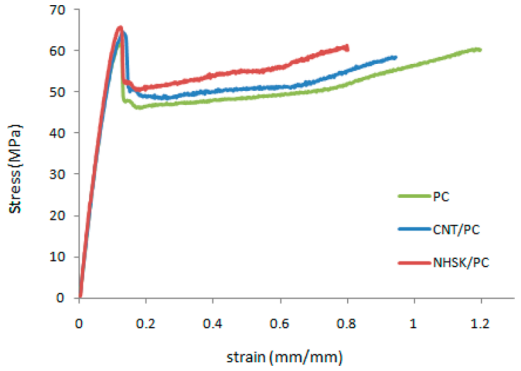

Figure 11. Stress–strain curves of polycarbonate (PC), CNT/PC, and NHSK/PC samples.

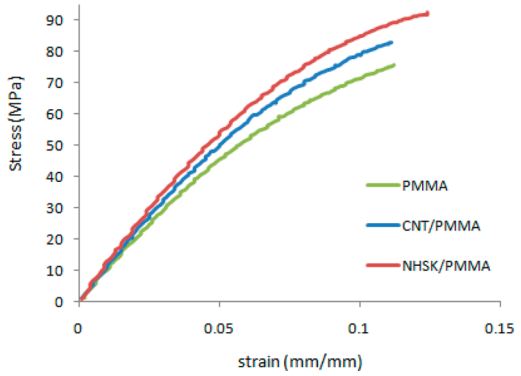

Figure 12. Stress–strain curves of PMMA, CNT/PMMA, and NHSK/PMMA samples.

CNT/PMMA. The ultimate tensile strength of NHSK/PMMA is 92.5 MPa compared with 75.8 MPa for PMMA and 82.7 MPa for CNT/PMMA. The trend is again consistent with the Raman results described earlier. The mechanical characterization data for all samples is summarized in Table 2, showing the impact of the NHSK structure on the modulus and ultimate strength of the nanocomposites.

Table 2. Mechanical Properties of the Samples

	Young's modulus (MPa)	ultimate tensile strength (MPa)
nylon-11	493	46.7
CNT/nylon-11	538	52.9
NHSK/nylon-11	586	59.1
PC	718	63.1
CNT/PC	735	64.7
NHSK/PC	791	65.8
PMMA	1031	75.8
CNT/PMMA	1107	82.7
NHSK/PMMA	1239	92.5

4. CONCLUSIONS

In summary, the motivation of this work is to pursue an approach that would allow one to modify and control the interfacial properties of a polymer nanocomposite via a non-covalent modification technique, the nanohybrid shish kebab structure, which does not introduce defects into the carbon nanotubes as is the case with chemical functionalization approaches. Differential scanning calorimetry and Raman spectroscopy were used to characterize the changes in the behavior of the interface due to the NHSK structure. It was found that the NHSK structure gave rise to higher melting points than the bulk nylon-11 polymer and that NHSK is more effective in improving the crystallinity of a nylon-11 matrix compared to the as-received CNTs. From the two melting points of the NHSK, a detailed structure of the NHSK is for the first time revealed to contain a uniform periodic inner crystal layer and lamellar kebabs, and a new growth model is hypothesized based on this structure. In Raman studies, due to the mismatch of coefficients of thermal expansion between the CNTs and the polymer, during sample heating the D* Raman band of the CNTs in the nanocomposite was observed to shift to lower wavenumbers as temperature was increased, indicating an increase in the tensile strain applied to the embedded CNTs. In addition, above a certain temperature the Raman peak was found to remain unchanged with respect to temperature, which was attributed to slip and a corresponding change in load transfer within the composite. In terms of the effectiveness of the reinforcement provided by the NHSK structure in the nylon-11 composite, we observed wavenumber shifts of the D* band of 0.32 cm^{-1} $°C^{-1}$ for the as-received CNT composite and 0.64 cm^{-1} $°C^{-1}$ for the NHSK nanocomposite over a 25 °C change in temperature. In addition, composites fabricated from amorphous polymers polycarbonate and PMMA, using both as-received CNTs and the NHSK structure, were also studied to investigate the mechanism by which the NHSK improves the interface between the CNTs and the polymer matrix. It was found that when the molecular compatibility between the matrix and the inclusions is sufficiently high, the mechanical interlocking effect is a further advantage in improving the interfacial load transfer. Mechanical tensile tests further indicate that the modulus and ultimate strength are improved by the presence of the NHSK structure, which demonstrates the interfacial load transfer between the CNTs and polymer matrices is enhanced and is consistent with the Raman spectroscopy results. These results show that the non-covalent NHSK nanostructure is able to provide a unique approach to effectively modify the properties of the interface between CNTs and polymers.

AUTHOR INFORMATION

Corresponding Author

*Phone: 201-216-8913. E-mail: frank.fisher@stevens.edu.

Notes

The authors declare no competing financial interest.

ACKNOWLEDGMENTS

We thank Dr. T. Su, Prof. X. Meng, Prof. H. Du, and J. Chi at Stevens for providing assistance with the use of the Raman spectrometer, Dr. T. Chou for assistance with electron microscopy, and D. Duenas for assistance with the NHSK experiments. Financial support for this work from the National Science Foundation (Grant No. 0846937) is gratefully acknowledged.

REFERENCES

(1) Moniruzzaman, M.; Winey, K. I. Polymer Nanocomposites Containing Carbon Nanotubes. *Macromolecules* **2006**, *39*, 5194–5205.
(2) Sahoo, N. G.; Rana, S.; Cho, J. W.; Li, L.; Chan, S. H. Polymer Nanocomposites Based on Functionalized Carbon Nanotubes. *Prog. Polym. Sci.* **2010**, *35*, 837–867.

(3) Rahmat, M.; Hubert, P. Carbon Nanotube-Polymer Interactions in Nanocomposites: A Review. *Compos. Sci. Technol.* **2011**, *72*, 72−84.
(4) Coleman, J. N.; Khan, U.; Blau, W. J.; Gun'ko, Y. K. Small but Strong: A Review of the Mechanical Properties of Carbon Nanotube-Polymer Composites. *Carbon* **2006**, *44*, 1624−1652.
(5) Ma, W.; Liu, L.; Zhang, Z.; Yang, R.; Liu, G.; Zhang, T.; An, X.; Yi, X.; Ren, Y.; Niu, Z.; Li, J.; Dong, H.; Zhou, W.; Ajayan, P. M.; Xie, S. High-Strength Composite Fibers: Realizing True Potential of Carbon Nanotubes in Polymer Matrix through Continuous Reticulate Architecture and Molecular Level Couplings. *Nano Lett.* **2009**, *9*, 2855−2861.
(6) Li, C. Y.; Li, L.; Cai, W.; Kodjie, S. L.; Tenneti, K. K. Nanohybrid Shish-Kebabs: Periodically Functionalized Carbon Nanotubes. *Adv. Mater.* **2005**, *17*, 1198−1202.
(7) Li, L.; Li, C. Y.; Ni, C. Polymer Crystallization-Driven, Periodic Patterning on Carbon Nanotubes. *J. Am. Chem. Soc.* **2006**, *128*, 1692−1699.
(8) Li, L.; Li, C. Y.; Ni, C.; Rong, L.; Hsiao, B. Structure and Crystallization Behavior of Nylon 66/Multi-Walled Carbon Nanotube Nanocomposites at Low Carbon Nanotube Contents. *Polymer* **2007**, *48*, 3452−3460.
(9) Li, L.; Li, B.; Hood, M. A.; Li, C. Y. Carbon Nanotube Induced Polymer Crystallization: The Formation of Nanohybrid Shish-Kebabs. *Polymer* **2009**, *50*, 953−965.
(10) Mago, G.; Kalyon, D. M.; Fisher, F. T. Nanocomposites of Polyamide-11 and Carbon Nanostructures: Development of Microstructure and Ultimate Properties Following Solution Processing. *J. Polym. Sci., Polym. Phys.* **2011**, *49*, 1311−1321.
(11) Liang, S.; Wang, K.; Chen, D.; Zhang, Q.; Du, R.; Fu, Q. Shear Enhanced Interfacial Interaction between Carbon Nanotubes and Polyethylene and Formation of Nanohybrid Shish-Kebabs. *Polymer* **2008**, *49*, 4925−4929.
(12) Zhang, S.; Lin, W.; Wong, C.-P.; Bucknall, D. G.; Kumar, S. Nanocomposites of Carbon Nanotube Fibers Prepared by Polymer Crystallization. *ACS Appl. Mater. Interfaces* **2010**, *2*, 1642.
(13) Li, B.; Li, L.; Wang, B.; Li, C. Y. Alternating Patterns on Single-Walled Carbon Nanotubes. *Nat. Nanotechnol.* **2009**, *4*, 358−362.
(14) Schadler, L. S.; Brinson, L. C.; Sawyer, W. G. Polymer Nanocomposites: A Small Part of the Story. *JOM* **2007**, *59*, 53−60.
(15) Ganesan, Y.; Peng, C.; Lu, Y.; Loya, P. E.; Moloney, P.; Barrera, E.; Yakobson, B. I.; Tour, J. M.; Ballarini, R.; Lou, J. Interface Toughness of Carbon Nanotube Reinforced Epoxy Composites. *ACS Appl. Mater. Interfaces* **2011**, *3*, 129−134.
(16) Cadek, M.; Coleman, J. N.; Barron, V.; Hedicke, K.; Blau, W. J. Morphological and Mechanical Properties of Carbon-Nanotube-Reinforced Semicrystalline and Amorphous Polymer Composites. *Appl. Phys. Lett.* **2002**, *81*, 5123−5125.
(17) Zhao, Q.; Wagner, H. D. Raman Spectroscopy of Carbon-Nanotube-Based Composites. *Philos. Trans. R. Soc. London, A* **2004**, *362*, 2407−2424.
(18) Liu, L.; Ma, P.-C.; Xu, M.; Khan, S. U.; Kim, J.-K. Strain-Sensitive Raman Spectroscopy and Electrical Resistance of Carbon Nanotube-Coated Glass Fibre Sensors. *Compos. Sci. Technol.* **2012**, *72*, 1548−1555.
(19) Ruan, S.; Gao, P.; Yu, T. X. Ultra-Strong Gel-Spun UHMWPE Fibers Reinforced Using Multiwalled Carbon Nanotubes. *Polymer* **2006**, *47*, 1604−1611.
(20) Frogley, M. D.; Zhao, Q.; Wagner, H. D. Polarized Resonance Raman Spectroscopy of Single-Wall Carbon Nanotubes within a Polymer under Strain. *Phys. Rev. B* **2002**, *65*, 113413.
(21) De la Vega, A.; Kinloch, I. A.; Young, R. J.; Bauhofer, W.; Schulte, K. Simultaneous Global and Local Strain Sensing in SWCNT-Epoxy Composites by Raman and Impedance Spectroscopy. *Compos. Sci. Technol.* **2011**, *71*, 160−166.
(22) Zhao, Q.; Wood, J. R.; Wagner, H. D. Using Carbon Nanotubes To Detect Polymer Transitions. *J. Polym. Sci., Polym. Phys.* **2001**, *39*, 1492−1495.
(23) Lourie, O.; Wagner, H. D. Evaluation of Young's Modulus of Carbon Nanotubes by Micro-Raman Spectroscopy. *J. Mater. Res.* **1998**, *13*, 2418−2422.
(24) Hadjiev, V. G.; Warren, G. L.; Sun, L.; Davis, D. C.; Lagoudas, D. C.; Sue, H.-J. Raman Microscopy of Residual Strains in Carbon Nanotube/Epoxy Composites. *Carbon* **2010**, *48*, 1750−1756.
(25) Wang, S.; Liang, R.; Wang, B.; Zhang, C. Load-Transfer in Functionalized Carbon Nanotubes/Polymer Composites. *Chem. Phys. Lett.* **2008**, *457*, 371−375.
(26) Eitan, A.; Fisher, F. T.; Andrews, R.; Brinson, L. C.; Schadler, L. S. Reinforcement Mechanisms in MWCNT-Filled Polycarbonate. *Compos. Sci. Technol.* **2006**, *66*, 1162−1173.
(27) Ma, P.-C.; Zheng, Q.-B.; Mader, E.; Kim, J.-K. Behavior of Load Transfer in Functionalized Carbon Nanotube/Epoxy Nanocomposites. *Polymer* **2012**, *53*, 6081−6088.
(28) Srivastava, I.; Mehta, R. J.; Yu, Z.; Schadler, L. S.; Koratkar, N. Raman Study of Interfacial Load Transfer in Graphene Nanocomposites. *Appl. Phys. Lett.* **2011**, *98*, 063102.
(29) Baibarac, M.; Baltog, I.; Lefrant, S. Raman Spectroscopic Evidence for Interfacial Interactions in Poly(bithiophene)/Single-Walled Carbon Nanotube Composites. *Carbon* **2009**, *47*, 1389.
(30) Hiemenz, P. C.; Lodge, T. P. *Polymer Chemistry*, 2nd ed.; CRC Press Inc.: Boca Raton, FL, 2007.
(31) Pennings, A. J.; van der Mark, J. M. A. A.; Kiel, A. M. Hydrodynamically Induced Crystallization of Polymers from Solution. *Kolloid-Z. Z. Polym.* **1970**, *237*, 336−358.
(32) Jiang, H.; Liu, B.; Huang, Y. Thermal Expansion of Single Wall Carbon Nanotubes. *J. Eng. Mater.* **2004**, *126*, 265−270.
(33) Mark, J. E. *Polymer Data Handbook*, 1st ed.; Oxford University Press: Oxford, U.K., 1999.
(34) Jiang, S.; Greiner, A.; Agarwal, S. Short Nylon-6 Nanofiber Reinforced Transparent and High Modulus Thermoplastic Polymeric Composites. *Compos. Sci. Technol.* **2013**, *87*, 164−169.